Published in IET Communications
Received on 30th November 2010
Revised on 22nd December 2011
doi: 10.1049/iet-com.2010.1054

In Special Section: Ultra-Wideband System Design, Signals and Coding

ISSN 1751-8628

Characterisation of ultra-wideband antenna arrays with spacings following a geometric progression

P.K. Gentner[1] *G.S. Hilton*[2] *M.A. Beach*[2] *C.F. Mecklenbräuker*[1]

[1]*Institute of Communications and Radio-Frequency Engineering, Vienna University of Technology, Gusshausstrasse 25/389, 1040 Vienna, Austria*
[2]*Centre for Communications Research, University of Bristol Merchant Venturers Building, Woodland Road, Bristol, UK*
E-mail: philipp.gentner@nt.tuwien.ac.at

Abstract: An ultra-wideband (UWB) antenna array is designed to satisfy given constraints in a (large) contiguous frequency range. Space limitations are tight in many applications and it is often infeasible to design the antenna array with preferred element spacings of $\lambda/2$ at the centre frequency. In this study, the authors compare uniform linear UWB antenna arrays and non-uniform reduced-aperture UWB antenna arrays with more compact element spacings following a geometric progression. The authors analyse and discuss performance degradations with respect to irregularly spaced monopoles. The manufactured non-uniform linear UWB antenna arrays are characterised by measurements in an anechoic chamber. The results are correlated with the arrayfactor and compared with measured data of uniform linearly spaced monopoles in the time and frequency domains. It is found that a compact non-uniform linear UWB array with element spacings following a geometric progression can be designed such that its main lobe performs very close to that of a uniform linear array, with an antenna array size reduction of 23.6% for a seven-element non-uniform linear UWB array.

1 Introduction

Recently, ultra-wideband (UWB) antennas have attracted increased interest; see [1–3]. This trend is driven by the approval of the IEEE 802.15.4a for implementation of both low- and high-data-rate communications, and by the need of multistandard wideband terminal antennas for plug and play devices for personal computers, notebooks and multi-media devices.

Beamforming [4] and beamsteering [5] can mitigate interference to other nodes and the signal-to-noise ratio at the destination node can be enhanced. For narrowband radio-frequency (RF) signals, beamforming and beamsteering can be realised by phased arrays, whereas for broadband RF signals true time-delay techniques have to be used if a near-optimal solution is needed. Malik *et al.* [6] have investigated sub-optimal solutions.

Our research focuses on small UWB monopoles and their use as antenna elements in arrays [7]. The monopoles we use have a size smaller than 0.25λ, whereas λ denotes the wavelength of the lowest-frequency point in UWB spectrum. For a physical antenna array it is interesting to know if the bandwidth of the array increases or decreases in terms of its radiation pattern response. The frequency range of our observation is in the FCC band [8] between 3 and 7 GHz. We explore a novel approach to the design and optimisation of UWB arrays and characterise the broadband beamforming behaviour. The array design considers a typical application scenario, where the antenna array structure acts as a UWB access point and is mounted under the ceiling of a room (see Fig. 1).

Wideband arrays with a constant element spacing will tend to produce unwanted grating lobes at higher frequencies. Arrays with log periodic spacings have been reported in literature, such as [9] and [10]. In this contribution, we analyse the wideband performance of a non-uniform linear array (NULA) using an alternative element spacing that follows a geometric progression. This linear array is introduced in Section 2, whereas the theoretic beampattern is calculated in Section 3 where the radiation pattern of the non-uniform array is compared with that of an uniform array; both arrays having isotropic radiating elements. In Section 4, measurement results are analysed and discussed for UWB antenna arrays with three, five and seven elements. The emitted fields are analysed in frequency and angle, as well as time against angle, as used in [11]. Additionally, we propose a correlation technique with the arrayfactor of an antenna array for benchmarking the broadband behaviour; this correlation technique has not been used and studied in literature for antenna arrays.

2 Antenna arrays under test

The antenna elements are small wideband monopoles [12] printed on an FR4 substrate. The size of one antenna is 18 mm × 28.1 mm. Each monopole is designed for a 50 Ω microstrip line impedance on a 1.5 mm-thick substrate.

Two antenna array designs are investigated: a uniform linear array (ULA) and an NULA with element spacings following a geometric progression. Exemplarily the NULA

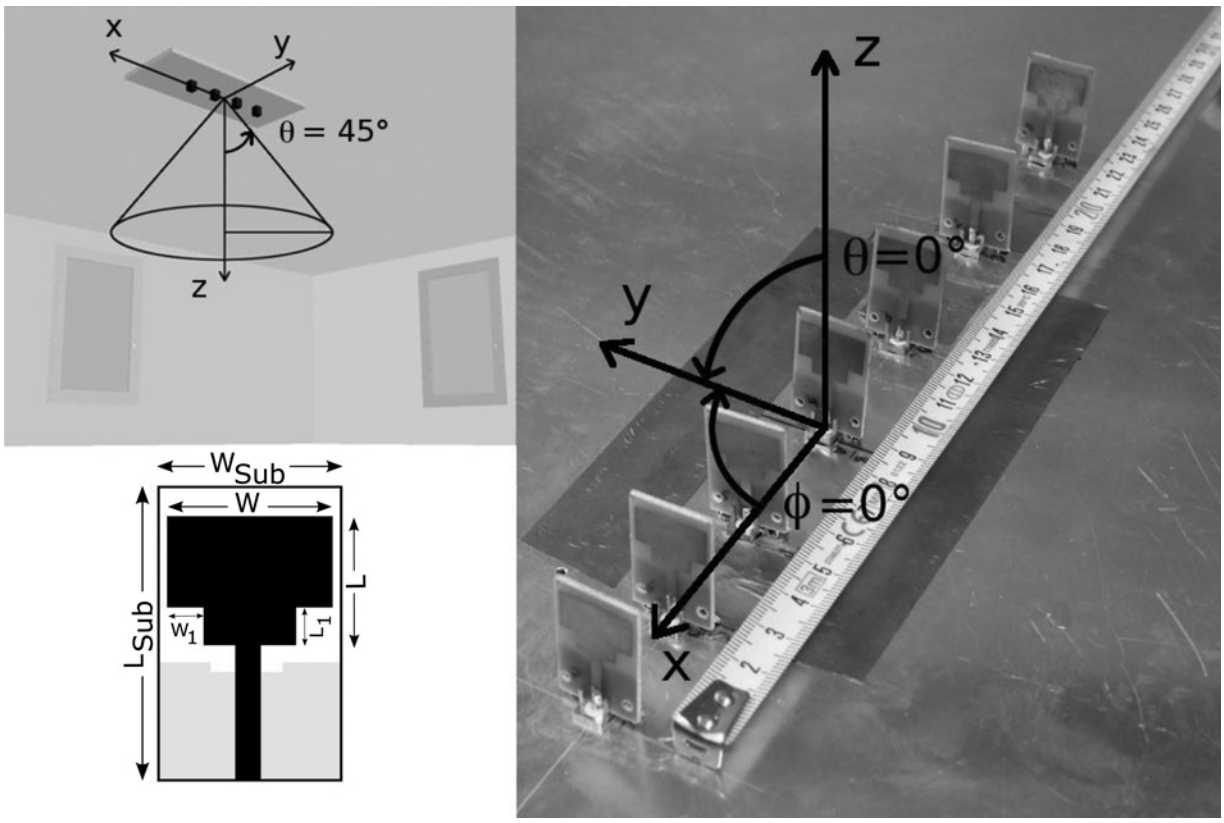

Fig. 1 *Photograph of a seven-element geometric wideband monopole array*

Top left: the application scenario for the array as an access point, mounted under the ceiling of a room is sketched. Bottom left: the wideband monopole antenna that are used as elements of the array with $W_{Sub} = 18$ mm, $L_{Sub} = 28.1$ mm, $W = 16$ mm, $L = 12.5$ mm, $W_1 = 3.5$ mm and $L_1 = 3.7$ mm)

with seven elements is shown in Fig. 1. For the ULA, each antenna element is positioned with constant $\lambda/2$ spacing to its neighbours. This spacing is calculated for the lowest operating frequency of the antenna element (5 cm for 3 GHz).

The geometric spacing is designed based on the following formulae

$$d_1 = \frac{\lambda_{max}}{2} \tag{1}$$

$$d_i = d_1 q^{i-1} \quad (i = 1, \ldots, N-1) \tag{2}$$

$$q = \sqrt[N-1]{\frac{\lambda_{min}}{\lambda_{max}}} \tag{3}$$

where N denotes the number of antenna elements. This geometric spacing takes into account both the lowest and highest operating frequencies.

All wideband antennas are mounted on an aluminium plate with a size of 700 mm × 400 mm shown in Fig. 1. The monopoles are connected to a feeding structure, which is placed behind the conducting plate to avoid coupling with the antenna elements. The feeding structure for the monopoles consists of a set of Wilkinson combiners. The way the combiner structure is used depended on the number of elements of the investigated array. For example, the NULA with five elements is fed with two 4-to-1 combiners and one 2-to-1 combiner, while the unused ports are terminated with 50 Ω loads.

The Wilkinson combiner structure [13] printed on an FR4 substrate is the bandwidth limiting component in the antenna array, because only one bended $\lambda/4$ section is used in the microstrip design. A transmission loss greater than 10 dB for frequencies above 6 GHz has been measured. Comparing the phase response of the laboratory prototype at the lowest and highest frequencies ($f_{min} = 3$ GHz and $f_{max} = 6$ GHz), the maximum phase difference among all combiner branches increases slightly with frequency, but does not exceed 20.2°.

With the limitations introduced by the combiner and the expected increased mutual coupling, at frequencies above 6 GHz, by adjacently positioned monopole elements, the geometric spacing is determined. Note that the smallest inter-element spacing is approximately equal to the size of one monopole element. The geometric distances are calculated with $f_{min} = c_0/\lambda_{max} = 3$ GHz and $f_{max} = c_0/\lambda_{min} = 6$ GHz (Table 1). The size reduction of the

Table 1 Inter-element spacings of the NULA following a geometric progression with quotient q

N	q	Inter-element spacing, mm						Array aperture, mm	Size reduction, %
		d_1	d_2	d_3	d_4	d_5	d_6	$\sum d_i$	Compared to $N{\cdot}\lambda_{max}/2$
3	0.7071	50	35.3	–	–	–	–	85.3	14.7
5	0.8409	50	42	35.3	29.7	–	–	157.0	21.5
7	0.8909	50	44.5	39.7	35.3	31.5	28.1	229.1	23.6

doi: 10.1049/iet-com.2010.1054

non-uniform geometric is calculated by comparing it to the uniform array. The reduction is 14.7% for the geometric linear array with three elements up to 23.6% for the seven-element array.

3 Theoretical discussion

In an ideal scenario the array factor of an N-element antenna array, containing isotropic elements, is given by

$$E_{\text{beam}}(\phi, f) = \frac{\sin(Nkd\sin\phi/2)}{N\sin(kd\sin\phi/2)} \tag{4}$$

with the wavenumber k and the inter-element spacing d. If the inter-element spacings d_i are non-uniform the array factor is calculated from

$$E_{\text{beam}}(\phi, f) = \frac{1}{N}\sum_{n=1}^{N} \mathrm{e}^{\mathrm{j}kr_n\cos\phi} \tag{5}$$

where $r_1 = 0$ and $r_n = \sum_{m=1}^{n-1} d_m$ for $n \geq 2$. Both formulae can be found in [14]. In Fig. 2, the array factors are calculated for the ULA and the NULA with $N = 3$ elements. The ULA is considered with a constant inter-element distance of 5 cm. The resulting antenna patterns are shown in decibels at the frequencies $f_{\min} = 3$ GHz and $f_{\max} = 6$ GHz. We see that the main lobes in broadside

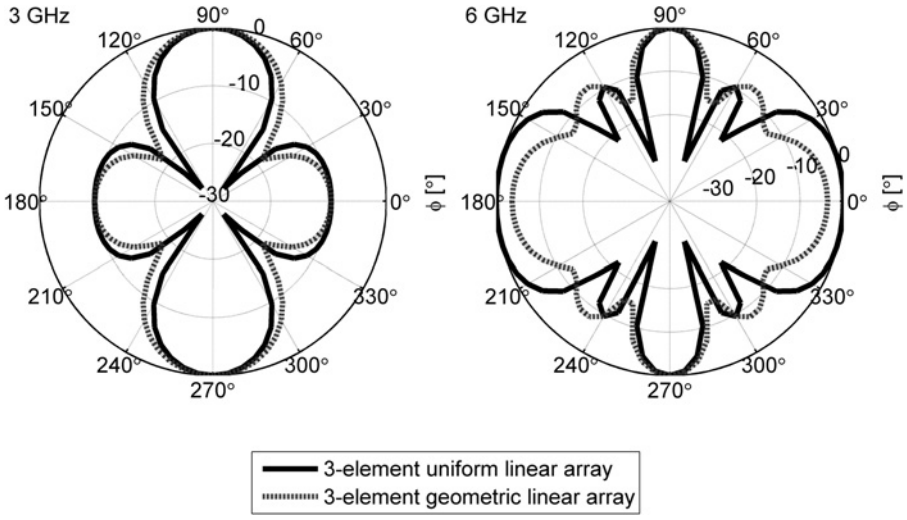

Fig. 2 *Antenna patterns for a three-element ULA and a three-element NULA with geometric spacing of isotropic elements*
Patterns are shown in decibels at the frequencies $f_{\min} = 3$ GHz and $f_{\max} = 6$ GHz

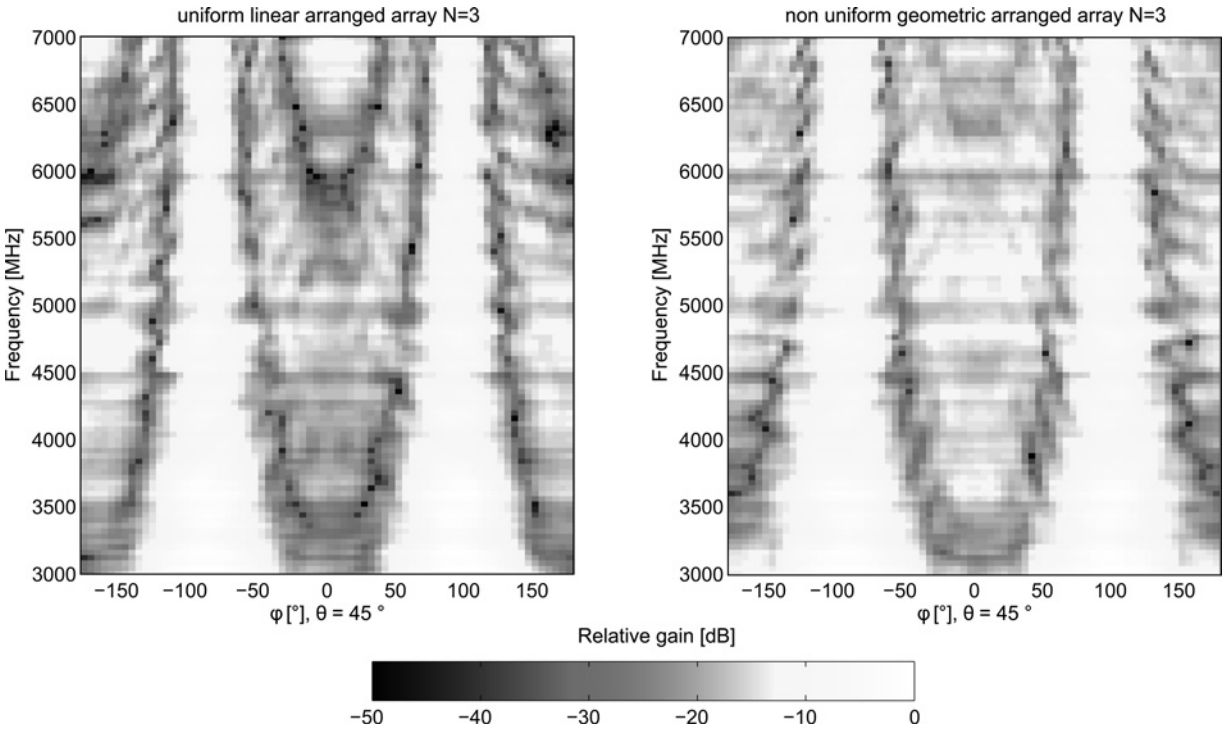

Fig. 3 *Frequency-resolved measurement of a three-element linear and geometric arrays*
In these figures the relative gain normalised to peak response is shown

orientation ($\phi = 90^\circ$ and $\phi = 270^\circ$) are similar in shape, but the 3 dB beamwidth for geometric spacing is 6° at 3 GHz, whereas it is only 3° at 6 GHz. Further, we note that the nulls of the ULA are approximately 10 dB deeper than for the array with geometric spacing. At 3 GHz the side lobes at endfire of the linear array ($\phi = 0^\circ$ and $\phi = 180^\circ$) and the side lobes of the geometric array are equal. At 6 GHz this behaviour differs; the grating lobes of the geometric array are 3.6 dB smaller compared to the ULA. From 6 GHz to higher frequencies the grating lobe in endfire splits up and moves towards the main lobe.

4 Measurement

In the first measurement, the antenna array under test consists of three monopole elements. The unused port of the 4-to-1 Wilkinson combiner is terminated with a 50 Ω load, and the whole array is mounted on the antenna positioner inside an anechoic chamber. The centre of the three-element array is placed in the origin of the coordinate system of the measurement set-up. A dual-polarised reference horn antenna from [15], is positioned in the farfield at a distance of 5.4 m (54 λ_{max}) from the array under test. In this study, we show measurements along azimuth ϕ at an elevation of $\theta = 45^\circ$ as defined in the coordinate system shown in Fig. 1. At this elevation angle the monopole angles are highly polarised to the reference horn antenna. For every azimuth ϕ, the network analyser measures the transmission coefficients over the frequency range from 3 to 7 GHz. The cable and combiner losses are subtracted from the measurements and normalised to the peak response.

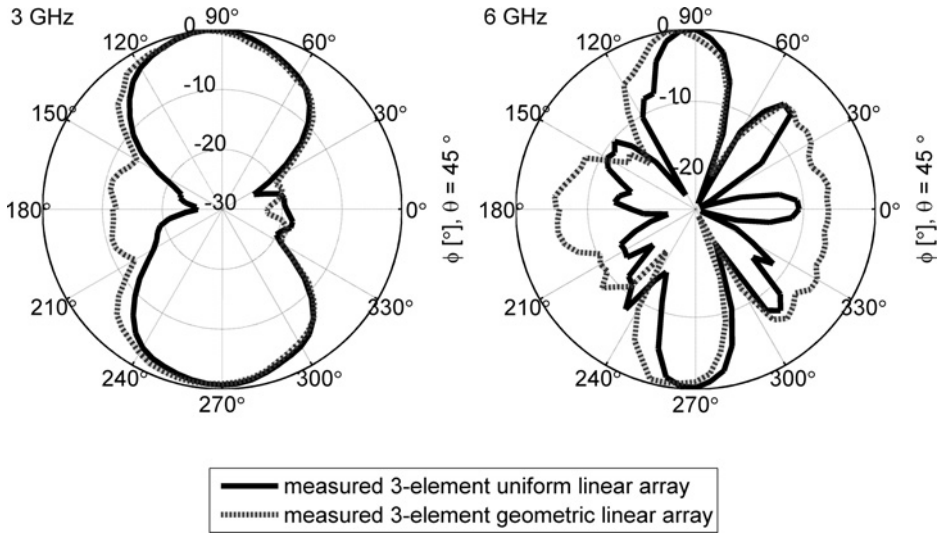

Fig. 4 *Measured radiation patterns of the three-element arrays at 3 and 6 GHz*
Radial scale in decibels is normalised to peak relative gain

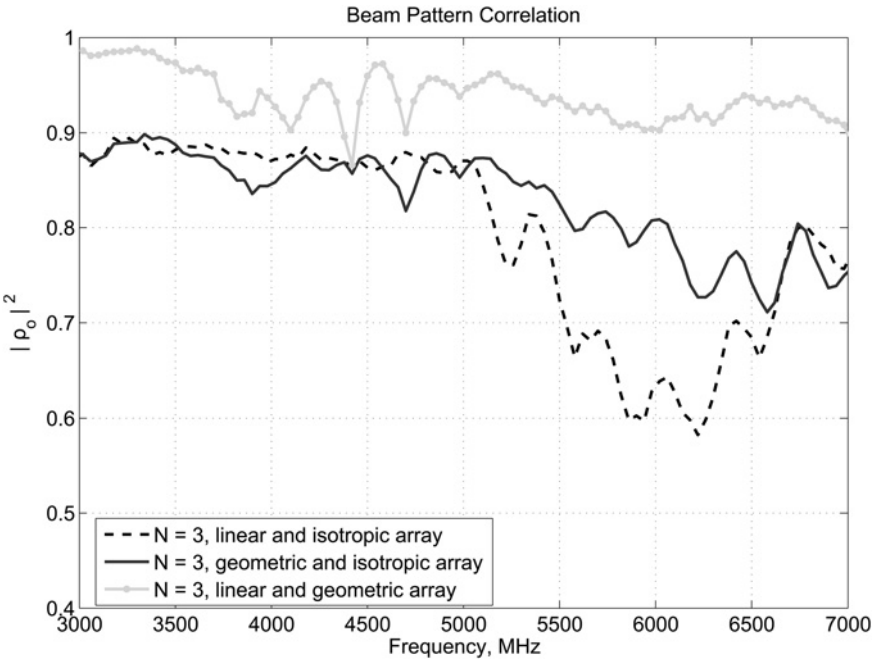

Fig. 5 *Correlation of the linear array factor with the measured data*
Correlation = 1 represents a perfect match between ideal isotropic antenna array and measured arrays at the observed plane

doi: 10.1049/iet-com.2010.1054

The result against frequency and azimuth ϕ is shown in Fig. 3, for the ULA on the left and the size reduced NULA on the right side, to visually compare the radiation patterns. The beamwidth of the main lobe ($\phi = \pm 90^\circ$) clearly narrows and the amplitude diminishes with increasing frequency for both arrays. Also side lobes at $\phi = 0^\circ$ appear in endfire orientation of both arrays at approximately 3.5 GHz, which move towards the main lobes with increasing frequency. For the left measurement, a null in the pattern appears at 6 GHz. This null is not observed in the measurements for the geometric array. We observe that the relative gain of the geometric array at endfire in the frequency range from 3 to 6 GHz is 6.48 dB greater in average than for the linear array and stays almost constant until approximately 6.5 GHz.

In Fig. 4, the measured radiation patterns for the three-element arrays are shown in a polar representation for the frequencies $f_{min} = 3$ GHz and $f_{max} = 6$ GHz. This is provided to directly compare the main lobes of the ULA and the NULA. The main lobes of the three-element array versions differ very little from each other at 3 GHz. For the higher frequency $f_{max} = 6$ GHz, we observe a shift in azimuth ϕ for the measured three-element arrays. The maximum shift of 15° is observed for the geometric spacing. This behaviour is caused by the frequency-dependent phase response of the combiner, which can be compensated when the array is used in applications where beamsteering or beamforming is applied. Side lobes are not visible in the polar representation for both arrays at 3 GHz, but do appear at higher frequencies. As previously mentioned, the side

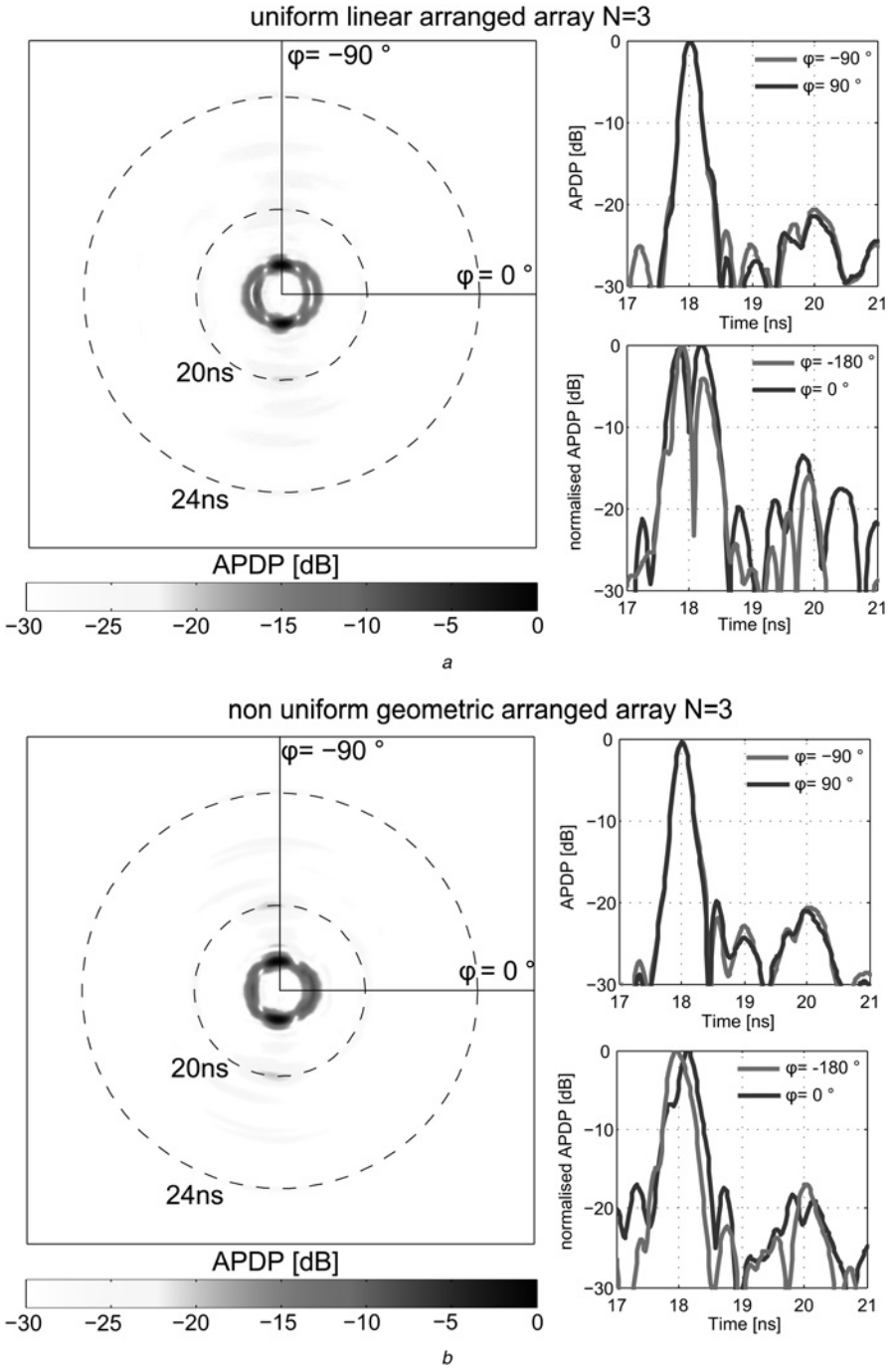

Fig. 6 *APDP of three-element ULA and NULA*
Decibel scale is relative to the pulse amplitude maximum

lobes in the 6 GHz measurement of the geometric array are larger, but show less nulls in endfire orientation.

To benchmark the designed antenna arrays over a wider-frequency range, we propose to use a correlation technique across the azimuth ϕ and frequency, which evaluates the similarities of the measured antenna patterns with the patterns of an idealised antenna array with isotropic elements. To the best of our knowledge this has not been used to compare antenna arrays. Following the authors in [16] and [17], we define the radiation pattern correlation ρ_{RP} as

$$\rho_{RP} = \frac{\int_{-\pi}^{\pi} |E(\phi, f)||E_{beam}(\phi, f)| d\phi}{\sqrt{\int_{-\pi}^{\pi} |E(\phi, f)|^2 d\phi \int_{-\pi}^{\pi} |E_{beam}(\phi, f)|^2 d\phi}} \quad (6)$$

For the idealised array with isotropic elements, equation (4) is used to calculate E_{beam}. The measured frequency- and angularly resolved complex data $E(\phi, f)$, as a field pattern of the tested antenna array, are correlated with the array factor for a three-element isotropic antenna array with a constant inter-element spacing of 5 cm. This radiation pattern correlation, with the copolarised emitted fields E_{beam} and $E(\phi, f)$, is shown in Fig. 5. In this representation, we note that the measured antenna arrays are similar to the isotropic response below 5 GHz. From 5 to 6.8 GHz, the linear array differs from the idealised isotropic case, mainly because of the unequal amplitude behaviour of the grating lobe at 6 GHz ($\lambda = d = 5$ cm). Higher-correlation values are observed for the comparison between the geometric and isotropic arrays, because the amplitude of the side lobes at

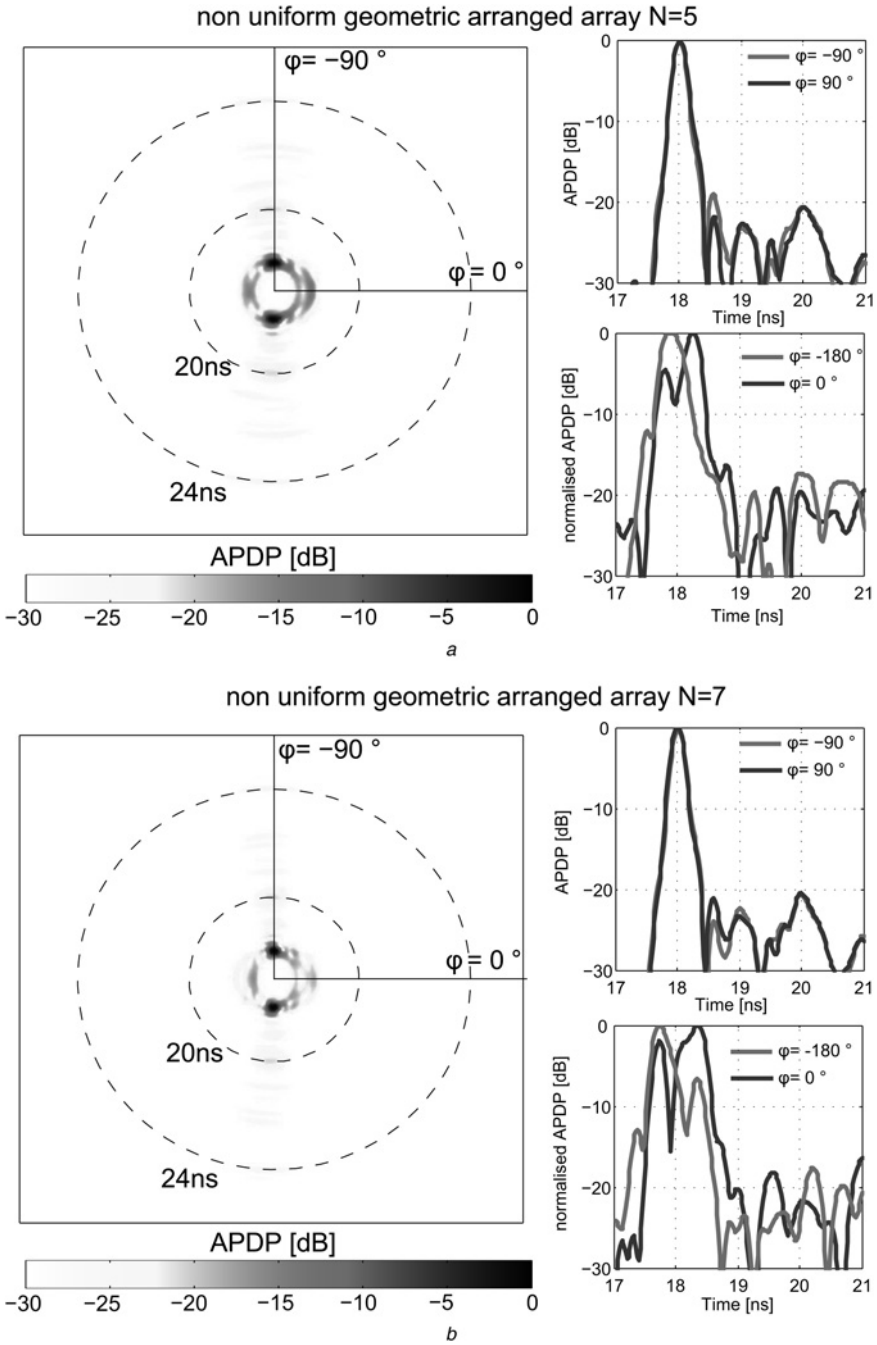

Fig. 7 *APDP of a five-element and a seven-element NULA*
Decibel scale is relative to the pulse amplitude maximum

doi: 10.1049/iet-com.2010.1054

$\phi = 0^\circ$ are higher, as shown in Fig. 3, and match with the grating lobes for the isotropic array. Of course, higher correlations are achieved by comparing the NULA with the ULA.

In our recent work [17], we defined the angular pulse-delay profile (APDP) as the inverse Fourier transform of the measured frequency- and angular-resolved antenna pattern. The measurement is interpolated in the time domain by zero-padding of the measured data before the transformation. The dimension of the resulting frequency-domain data vector is increased by a factor of four. Thereafter, a Hann window is applied to reduce leakage effects.

In Fig. 6, the APDP in decibels is shown for the three-element ULA in part *a* and for the NULA in part *b*. The diagrams are normalised to the pulse maximum which occurs at the measurement distance of 5.4 m leading to a temporal delay of 18 ns. Pulse features at a constant propagation delay are situated on a circle around the origin in this figure. The azimuth ϕ has the same meaning as in a polar radiation pattern diagram. The origin of the diagram is set to a delay time of 17 ns. In the colour-coded diagrams, pulse envelopes are shown, which are radiated from the antenna array in the reverse ($\phi = -90^\circ$) and front directions ($\phi = 90^\circ$). The APDP of the broadside and endfire direction ($\phi = 0^\circ$ and $\phi = \pm 180^\circ$) is plotted against time for the ULA and NULA, where in endfire the measurements are normalised to the maximum of the pulse envelope.

Comparing the 3 dB pulse-beam width at $\phi = 90^\circ$, we note that the pulse-beam width of the array with geometric spacings is 6.8° wider than the one of the ULA. In endfire (0°) pulse maximas are clearly visible but smaller in amplitude than the pulse envelope at broadside. For the ULA this amplitude difference of 12.8 dB is measured and for the NULA this is 8 dB. The 3 dB pulse envelope duration to the front of the ULA is found to be equal to the NULA with 220 ps. Clearly, the pulse envelope duration increases towards the endfire. In contrast to the geometric array, the uniform array shows a local minimum at $\phi = 0^\circ$ inside the pulse envelope between 17.6 and 18.5 ns. This minimum is created by the distorted spectrum (appearing and disappearing side lobes/grating lobes in the frequency domain) in the endfire orientation shown in Fig. 3. The beam tilt, which is introduced by the feeding network, is also clearly observable in the colour-coded diagrams. The pulse envelope in endfire of the NULA is more than 160 ps smaller (at −10 dB normalised APDP and ignoring local minima of the ULA) than that of the ULA. This is explained by the reduced aperture of the NULA.

The analysis is extended to five- and seven-element NULAs. Measurement results are shown in the time domain for the five-element NULA in part *a* and for the seven-element NULA in part *b* of Fig. 7. For this measurement, two 4-to-1 and one 2-to-1 Wilkinson combiners are used. The unused ports are terminated with 50 Ω loads. As expected, the angular beam width decreases with increasing number of array elements. The 3 dB pulse-beam width at $\phi = 90^\circ$ is 21° observed for the five-element array and 15° for the seven-element array. In endfire, the pulse envelope

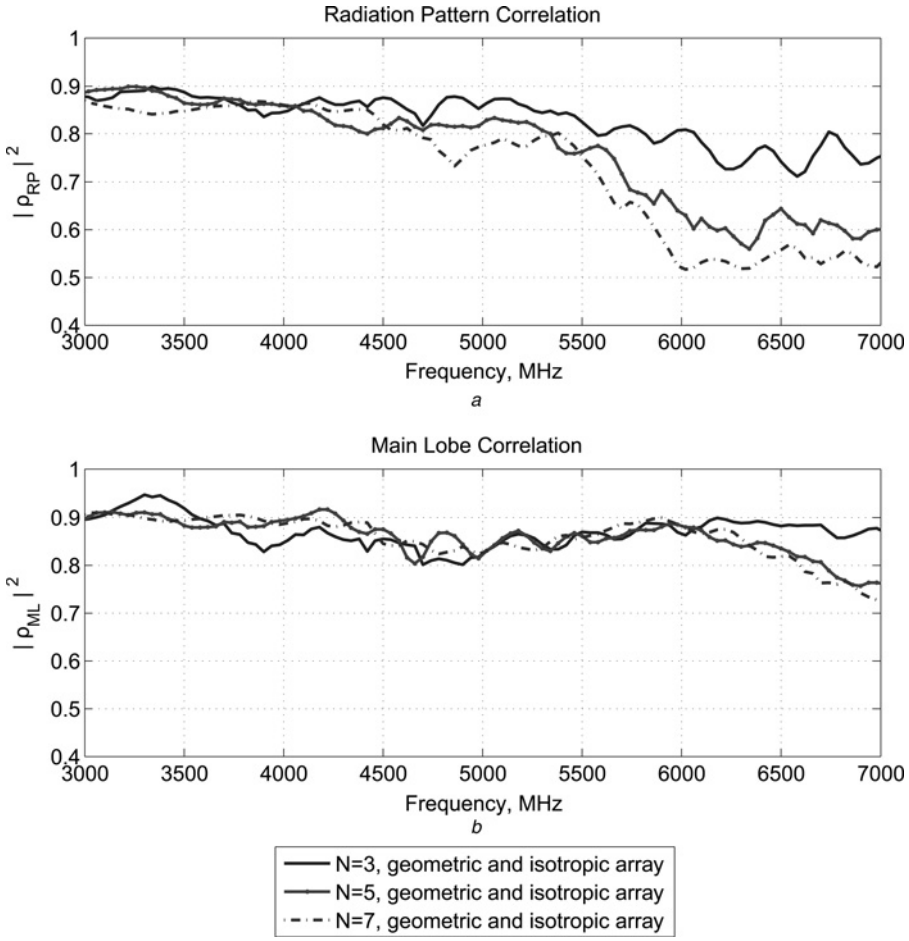

Fig. 8 *Correlations for the three-, five- and seven-element NULAs*

a In the top diagram, correlation of the geometric arrays with the beampattern created by the isotropic elements
b In the bottom, only a main lobe correlation is performed

amplitude decreases with increasing number of array elements. Comparing the pulse-delay amplitude at broadside and endfire, the difference is 13.4 dB for the five-element array and 18.2 dB seven-element array. The width of the envelope in direction of $\phi = 0^\circ$ also increases. This can be explained by the coherent superposition of N-transmitted pulses by N-monopole antennas.

The radiation pattern correlations defined in (6) for the three-, five- and seven-element NULAs are shown in Fig. 8*a*. Between 3 and 5 GHz the negative gradient of the similarity value increases with the number of elements in the array. At frequencies above 6 GHz the designed arrays differ significantly from the isotropic array because of lower grating lobe levels. In general, the number of side lobes increases with the number of isotropic elements in an array. Also, the side lobe level increases up to the frequency at which grating lobes appear (at λ distance). The wideband monopoles used in the geometric array, do not produce as many sidelobes as the isotropic array. For this reason, the similarity decreases with increasing frequency up to 6 GHz and increasing number of elements. An increasing size reduction of the array, given with an increasing number of elements for the NULAs, leads to a decreasing frequency range of radiation pattern similarity.

In Fig. 8*b*, the main lobe correlations ρ_{ML} defined as

$$\rho_{\mathrm{ML}} = \frac{\int_{-\pi}^{\pi} |E(\phi, f)||E_{\mathrm{beam}}(\phi, f) \sin \phi| \mathrm{d}\phi}{\sqrt{\int_{-\pi}^{\pi} |E(\phi, f)|^2 \mathrm{d}\phi \int_{-\pi}^{\pi} |E_{\mathrm{beam}}(\phi, f) \sin \phi|^2 \mathrm{d}\phi}} \quad (7)$$

for the three-, five- and seven-element NULAs are shown. The weighting factor $\sin \phi$ in (7) reduces the influence of the high grating lobe levels of the isotropic array on the correlation value. This is done for showing directly the main lobe similarities between the manufactured NULA and the corresponding ideal ULA with isotropic elements. The main lobe of the NULAs are similar over a large-frequency range up to 7 GHz compared to the isotropic arrays. In the measured frequency-resolved results (see Fig. 3), the relative gain decreases with frequency. We note that the main lobe finally deteriorates in the frequency range between 8 and 10 GHz. At 5 GHz the main lobe correlation for all measured NULAs shows a dip in correlation. This is caused by the used Wilkinson combiners, which have a 3 dB ripple in the transmission coefficient in this frequency range.

5 Conclusions

In this paper, we have proposed and analysed the design and characterisation of UWB NULAs with element spacings follow a geometric progression. The measured behaviour of manufactured antenna arrays in both the time and frequency domains has been discussed. Additionally, for quantitative evaluation of the array measurements, we introduce a correlation technique specifically designed for UWB antenna arrays to facilitate interpretation and comparison. The characterised UWB antenna array with geometric spacing is reduced in size up to 23.6% for a seven-element array compared to a $\lambda/2$-spaced array. For the laboratory prototype the compact irregular spaced array provides similar performance in terms of main lobe radiation pattern to an ideal isotropic antenna array. However, the performance is found to decrease with an increasing number of antenna elements. Finally, we note that the correlation technique detects antenna array effects, such as appearing or disappearing of side lobes or grating lobes in the frequency domain.

6 References

1 Chen, Z.N., See, T.S.P., Qing, X.: 'Small printed ultrawideband antenna with reduced ground plane effect', *IEEE Trans. Antennas Propag.*, 2007, **55**, (2), pp. 383–388

2 Guo, L., Wang, S., Chen, X., Parini, C.: 'A small printed quasi-self-complementary antenna for ultrawideband systems', *IEEE Antennas Wirel. Propag. Lett.*, 2009, **8**, pp. 554–557

3 Hwang, J.-N., Soergel, W., Wiesbeck, W.: 'Periodical protrusions for UWB slot antennas'. Proc. German Microwave Conf., GEMIC, March 2006

4 Ries, S., Kaiser, T.: 'Highlights of UWB impulse beamforming'. EUSIPCO 13, September 2005

5 Hashemi, H., Chu, T.-S., Roderick, J.: 'Integrated true-time-delay-based ultra-wideband array processing', *IEEE Commun. Mag.*, 2008, **46**, (9), pp. 162–172

6 Malik, W.Q., Allen, B., Edwards, D.J.: 'A simple adaptive beamformer for ultrawideband wireless systems'. Proc. IEEE 2006 Int. Ultra-Wideband Conf., 2006, pp. 453–457

7 Saleeb, A.: 'Smart antenna techniques applied to UWB array antennas'. The Institution of Engineering and Technology Seminar on Ultra Wideband Systems, Technologies and Applications, 2006, April 2006, pp. 239–243

8 Federal Communications Commission: 'Revision of part 15 of the commission's rules regarding ultra-wideband transmission systems'. First Report and Order, April 2002

9 Hall, P.: 'Multioctave bandwidth log-periodic microstrip antenna array', *IEE Proc.*, 1986, **133**, (2), pp. 127–136

10 Hochwald, B.M., Maretta, T.L.: 'Adapting a downlink array from uplink measurements', *IEEE Trans. Signal Process.*, 2002, **49**, (3), pp. 642–653

11 Soergel, W., Waldschmidt, C., Wiesbeck, W.: 'Transient radiation from a linear UWB antenna array'. Int. Symp. on Electromagnetic Theory, URSI EMTS, May 2004, pp. 1254–1255

12 Jung, J., Choi, W., Choi, J., *et al.*: 'A small wideband microstrip-fed monopole antenna', *IEEE Microw. Wirel. Compon. Lett.*, 2005, **15**, (10), pp. 703–705

13 Pozar, D.-M.: 'Microwave engineering' (Wiley, 1997, 2nd edn.), Ch. 7.3

14 Balanis, C.: 'Antenna theory: analysis and design' (Wiley, 1997, 2nd edn.), Ch. 6.3

15 Hilton, G.S., Urwin-Wright, P.R., Craddock, I.J.: 'Full radiation pattern measurements of antenna arrays to obtain accurate pattern correlation levels for use in MIMO system performance'. Proc. IEE Antenna Measurements and SAR AMS 2004, 2004, pp. 83–86

16 Vaughan, R.G., Andersen, J.B.: 'Antenna diversity in mobile communications', *IEEE Trans. Veh. Technol.*, 1987, **36**, (4), pp. 149–172

17 Gentner, P., Hilton, G., Beach, M., Mecklenbräuker, C.: 'Near and farfield analysis of ultra wideband impulse radio beamforming in the time domain'. 2010 IEEE Int. Conf. on Ultra-Wideband (ICUWB), September 2010, vol. 2, pp. 1–4

doi: 10.1049/iet-com.2010.1054